

Three-Dimensional Model for the Crust and Upper Mantle in the Barents Sea Region

PAGES 160–161

The Barents Sea and its surroundings is an epicontinental region which previously has been difficult to access, partly because of its remote Arctic location (Figure 1) and partly because the region has been politically sensitive. Now, however, this region, and in particular its western parts, has been very well surveyed with a variety of geophysical studies, motivated in part by exploration for hydrocarbon resources. Since this region is interesting geophysically as well as for seismic verification, a major study [Bungum *et al.*, 2004] was initiated in 2003 to develop a three-dimensional (3-D) seismic velocity model for the crust and upper mantle, using a grid density of 50 km.

This study, in cooperation between NORSAR, the University of Oslo (UiO), and the U.S. Geological Survey (USGS), has led to the construction of a higher-resolution, regional lithospheric model based on a comprehensive compilation of available seismological and geophysical data. Following the methodology employed in making the global crustal model CRUST5.1 [Mooney *et al.*, 1998], the new model consists of five crustal layers: soft and hard sediments, and crystalline upper, middle, and lower crust. Both *P*- and *S*-wave velocities and densities are specified in each layer. In addition, the density and seismic velocity structure of the uppermost mantle, essential for *Pn* and *Sn* travel time modeling, are included.

The general motivation for developing this model is basic geophysical research. A more specific goal is to create a model for research on the identification and location of small seismic events in the study region, and for operational use in locating and characterizing all seismic events in the region. Along with the development of the model, a calibration and validation program is also included, aimed at quality controlling the model through comparisons between observed and synthetic travel times, and at improving regional event locations.

The study area is shown in Figure 1. The principle grid points of the velocity model are shown, with 1490 nodes spaced 50 km apart. The input database consists of 712 1-D velocity-depth profiles that are based on various kinds of surveys, including onshore and offshore wide-angle experiments, and density modeling along deep seismic reflection profiles with subsequent density-to-velocity conversion. Most of the data sets are published as 2-D crustal velocity cross sections, and these were sampled every 25 km to obtain the 1-D velocity-depth profiles.

For each of the grid points in Figure 1, the lithosphere is represented by two sedimentary layers separated at a *P*-wave velocity of 3.0 km/s, while the crystalline crust consists of an upper, a middle, and a lower part that are separated at 6.0 and 6.5 km/s, respectively (6.5 and 7.0 km/s for oceanic crust). The upper mantle velocity is also specified at each grid point. Values for each of the tiles located along the wide-angle profiles (Figure 1) are constrained based on primary data.

For regions not constrained by primary data, an interpolation scheme was developed, based on the definition of geological provinces that are characterized by individual tectono-sedimentary histories. Analyses of the compiled database demonstrated strong correlations between sediment thickness and the thickness of the crystalline basement within each of the continental provinces. Depth-to-base ment maps were compiled to use this quantitative correlation as a basis for filling the unconstrained nodes. Within each geological

province and each of the crustal layers, the velocities are fixed and represented by a mean value calculated from the velocity database. This scheme is valid for at least 80% of the target region, but is not applicable within the oceanic crustal domain, sediment-free cratons, and regions overprinted by convergent tectonics. For these areas, a simple nearest-neighbor interpolation is applied.

An alternative interpolation approach applies a continuous curvature gridding algorithm for horizontal interpolation of seismic velocities within each of the defined provinces. Both of these approaches will be tested in terms of travel time modeling and calibration to explore their potentials and limitations with respect to seismic velocity model construction.

To provide a complete lithospheric model, the crustal model was complemented with an upper mantle velocity structure based on the work of Shapiro and Ritzwoller [2002], thereby covering depths sufficient for the tracing of far-regional wave paths. The final representation of the 3-D model will include depth maps for the interfaces and the lateral velocity variation within each layer. For example, the depth to Moho varies from 4 to 5 km (including 2-km water column) off western Svalbard (see Figure 1) to 54 km below the northern Scandinavian craton. The *P*-wave velocities below the Moho range from 7.4 km/s west of Svalbard to

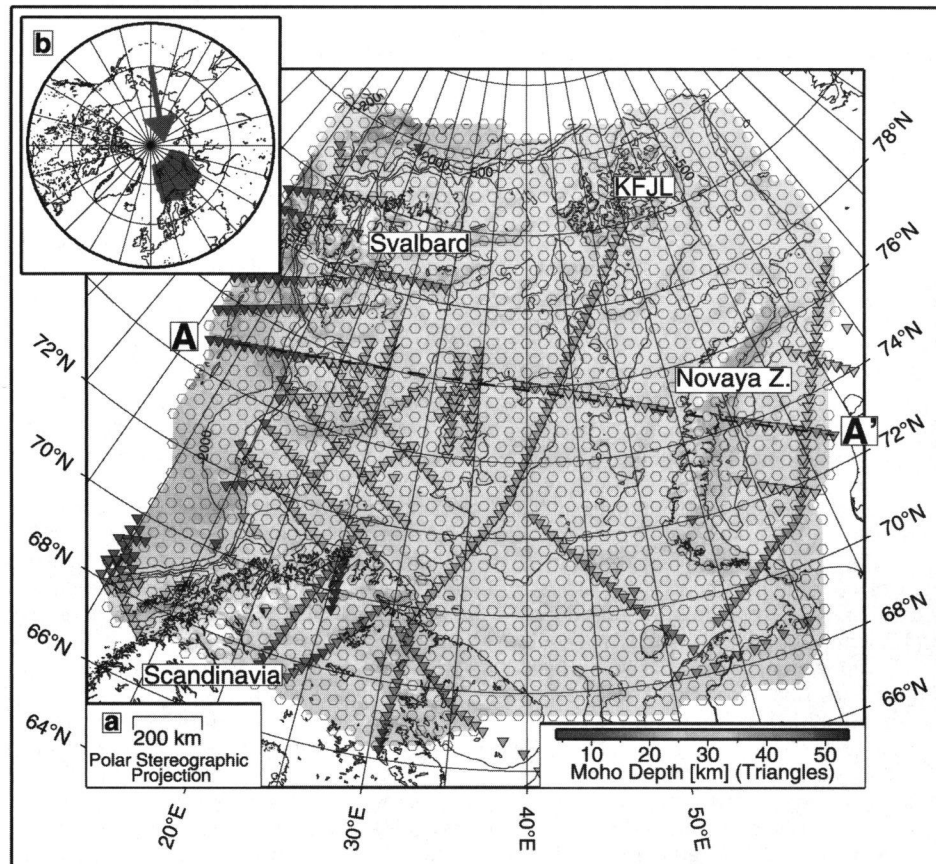


Fig. 1. Map of the greater Barents Sea region, shown in red in the inset map. The lines marked with triangles are wide-angle profiles where the color coding indicates the Moho depth. The small hexagons are tiles spaced 50 km apart that will be filled with crustal and upper mantle velocities. The profile A-A' is the one for which detailed results are shown in Figure 2. KFJL, Kaiser Franz Josef Land. Original color image appears at the back of this volume.

8.35 km/s below Scandinavia.

Figure 2 shows an example of a set of geological and geophysical data compiled in this study along the 1800-km-long, west-east transect A-A' in Figure 1. Figure 2a shows a cross section along A-A', and incorporates most of the geophysical data available. The thickness of the sedimentary cover in the Barents/Kara Sea regions may exceed 20 km. Late Permian to Early Triassic convergent movements along southwestern Novaya Zemlya (the Uralian orogeny; see Figure 1) resulted in uplift and subsequent erosion of sedimentary rocks. Currently, Middle to Late Paleozoic rocks outcrop on Novaya Zemlya.

The velocity structure of the crystalline crust and the Moho topography is well known (solid line) from Norwegian and Russian contributions [e.g., Breivik *et al.*, 2002; Sakoulina *et al.*, 2003]. Whereas the depth to Moho to the west of the continent-ocean transition (COT) exhibits local variations, the lower crystalline crust is rather homogeneous with a velocity of 6.8 km/s.

A closer view of the COT along the transect (Figure 2b) [Breivik *et al.*, 2002] presents the detailed 2-D seismic velocity structure derived from wide-angle profiles in the target region. Almost every profile of the input database is available as a continuous 2-D velocity cross section as is shown here. This was achieved either by obtaining digital models or by digitizing published contour plots. The interpretation of seismic velocities was facilitated in particular by deep seismic reflection lines, which are available especially for the western Barents Sea region. Figure 2c shows a data example with a prominent crustal root structure (arrows), and Figure 2b a line drawing of the entire line [e.g., Gudlaugsson *et al.*, 1987].

Regional potential-field data taken along transect A-A' reveal features that support the geological interpretation (Figure 2d). The comparison of the free-air gravity field with the field calculated from the model will be part of its final validation. Figure 2e shows seismic wave fronts (black, 5 s steps) and rays (white) from an initial first arrival travel time modeling using a finite difference method, and Figure 2f compares the corresponding travel time curve (black) with the 1-D models IASPEI91 (blue [Kennett and Engdahl, 1991]) and BAREY (red [Schweitzer and Kennett, 2002]). Reflecting the large lateral inhomogeneities along these profiles, the figure shows significant deviations from the 1-D travel time models, albeit, as expected, a lot less for the regional model (BAREY) than for the global model (IASPEI91).

Validation of the velocity model includes forward modeling of observed travel times and relocation of seismic events. For this purpose, a set of reference events with known or well-located epicenters was compiled. Such events are referred to as "ground truth" (GT) events. These events are taken from Hicks *et al.* [2004] and Bondar *et al.* [2004], supplemented by additional data from NORSAR.

The GT events comprise quarry blasts located mainly in Scandinavia and the Kola Peninsula, nuclear explosions in NW Russia and on Novaya Zemlya, and natural earthquakes. With these events, good travel path coverage is

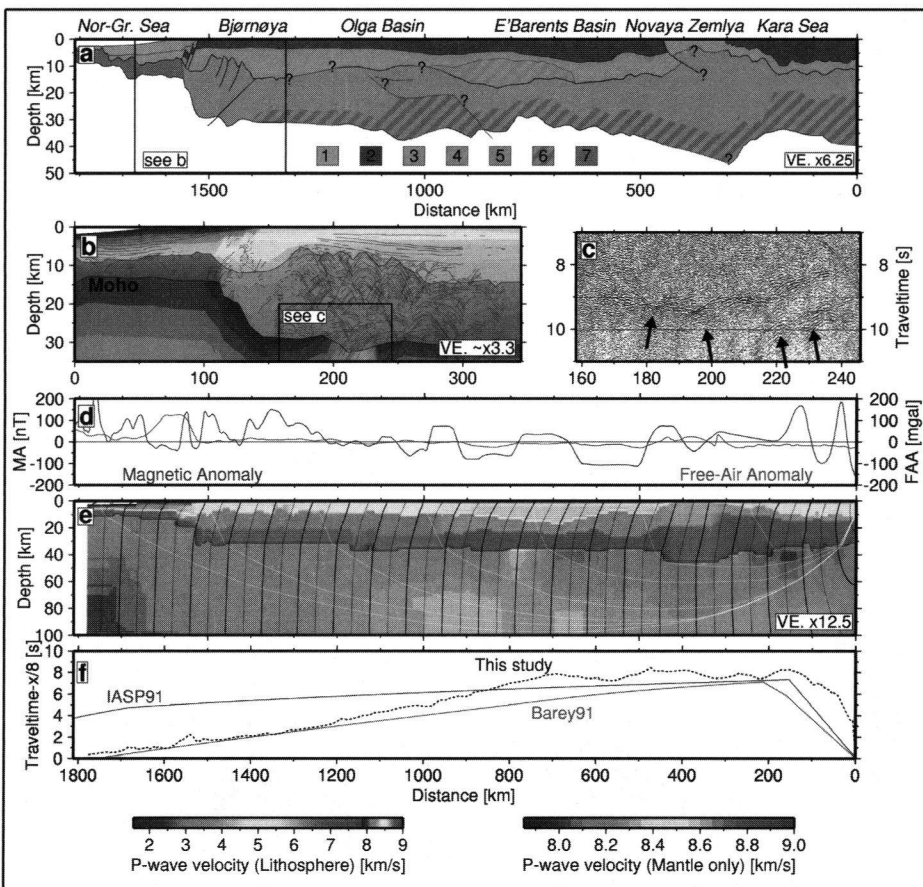


Fig. 2. Observations, interpretations, and modeling for the Barents Sea A-A' transect shown in Figure 1. Figure 2a shows the geological units along the transect ranging from the oceanic crustal domain in the very west to Novaya Zemlya and the Kara Sea in the east. Along the 1800-km-long transect, all available data were used to display the distribution of sedimentary and crystalline crustal rocks: 1, Cenozoic sediments; 2, Mesozoic sediments; 3, Paleozoic sediments; 4, Paleozoic sediments and/or crystalline rocks; 5, continental crystalline rocks; 6, lower crustal crystalline rocks with v_p 6.6–6.8 km/s; and 7, oceanic crystalline rocks. Figures 2b and 2c illustrate database examples along this transect, i.e., a P-wave velocity model (with line drawing) and deep seismic reflection data, respectively (see insert boxes for along-transect location). Figure 2d shows potential-field data along the profile, Figure 2e shows the 3-D model with superimposed seismic wave fronts, and Figure 2f shows travel times in comparison with two 1-D models. For the velocity models in Figures 2b and 2e, the lower color scales apply, where the left scale covers the entire range of lithospheric velocities and the right scale covers the mantle velocities only. Note that at 7.8 km/s, the scale shows repeating colors (crust-mantle transition). Original color image appears at the back of this volume.

obtained in the western half of the model region and in the SE Barents Sea. The coverage is weaker to the NE, due to a lack of recorded seismicity and man-made events from that part of the target region.

This new model of the crust and upper mantle in the greater Barents Sea region is now undergoing further refinement and will be completed by the end of 2005. Documentation of the model and insights into the structure and evolution of the Barents Sea region will be published in forthcoming papers, and the final model will be made available for use by the scientific community.

Acknowledgments

We thank Anatoli Levshin for providing the Shapiro and Ritzwoller [2002] mantle velocity model, and William S. Leith and Johannes Schweitzer for their valuable contributions. This research has been sponsored by the U.S.

Department of Energy under contracts DE-FC52-03NA995081, DE-FC52-03NA995092, and DE-FC52-03NA995313.

References

- Bondar, I., et al. (2004), Collection of a reference event set for regional and teleseismic calibration, *Bull. Seismol. Soc. Am.*, 94(4), 1528–1545.
- Breivik, A. J., R. Mjelde, P. Grogan, H. Shimamura, Y. Murai, and Y. Nishimura (2003), Crustal structure and transform margin development south of Svalbard based on ocean bottom seismometer data, *Tectonophysics*, 369, 37–70.
- Bungum, H., O. Ritzmann, J. I. Faleide, N. Maercklin, J. Schweitzer, W. D. Mooney, S. T. Detweiler, and W. S. Leith (2004), Development of a three-dimensional velocity model for crust and upper mantle of the Barents Sea, Novaya Zemlya, Kara Sea and Kola-Karelia Regions, paper presented at Trends in Nuclear Explosion Monitoring: 26th Seismic Research Review, Natl. Nucl. Secur. Admin., Orlando, Fla., 21–23 Sept.

- Gudlaugsson, S.T., J.I. Faleide, S. Fanavoll, and B. Johansen (1987), Deep seismic reflection profiles across the western Barents Sea, *Geophys. J.R. Astron. Soc.*, 89, 273–278.
- Hicks, E. C., T. Kvaerna, S. Mykeltveit, J. Schweitzer, and F. Ringdal (2004), Travel-times and attenuation relations for regional phases in the Barents Sea region, *Pure Appl. Geophys.*, 161, 1–19.
- Kennett, B. L. N., and E. R. Engdahl (1991), Travel times for global earthquake location and phase identification, *Geophys. J. Int.*, 105, 429–465.

- Mooney, W.D., G. Laske, and T.G. Masters (1998), CRUST 5.1: A global crustal model at $5^\circ \times 5^\circ$, *J. Geophys. Res.*, 103(B1), 727–747.
- Sakoulina, T.S., Y.V. Roslov, and N.M. Ivanova (2003), Deep seismic investigations in the Barents and Kara seas, *Izv. Russ. Acad. Sci. Phys. Solid Earth*, 39(6), 438–452.
- Schweitzer, J., and B.L.N. Kennett (2002), Comparison of location procedures—The Kara Sea event of 16 August 1997, Semianual Technical Summary, NORSAR Sci. Rep. No. 1-2002, Kjeller, Norway.

- Shapiro, N.M., and M.H. Ritzwoller (2002), Monte-Carlo inversion for a global shear velocity model of the crust and upper mantle, *Geophys. J. Int.*, 151, 88–105.

Author Information

H. Bungum, NORSAR, Kjeller, Norway; O. Ritzmann, University of Oslo, Norway; N. Maercklin, NORSAR, Kjeller, Norway; J.-I. Faleide, University of Oslo, Norway; and W.D. Mooney and S.T. Detweiler, U.S. Geological Survey, Menlo Park, Calif.

NEWS

RADARSAT-1 Interferometric Baseline Catalog at the Alaska Satellite Facility

PAGE 158

Interferometric synthetic aperture radar (InSAR) techniques are used in numerous applications, especially in long-term monitoring of surface deformations. For these studies, a large data volume is needed and the issue of careful data selection is critical. One of the main parameters to decide whether a particular data set is suitable for a certain application is the interferometric baseline. The knowledge of the baselines limits the extra processing efforts required to determine the usefulness of data sets for the application project.

While the European Space Agency (ESA) makes available the interferometric baseline information for the ESA Remote-Sensing Satellites (ERS) 1 and 2 and the Envisat satellite, the baseline information for the Canadian Space Agency's RADARSAT-1 satellite is not available. With the development of the RADARSAT-1 baseline catalog at the Alaska Satellite Facility (ASF) in the University of Alaska Fairbanks' Geophysical Institute, this knowledge gap is closed.

RADARSAT-1 acquires data at different look angles that define the various beam modes. An interferometric image pair consists of two SAR images acquired in the same beam mode with almost identical image geometry. The repeat-pass geometry for the RADARSAT-1 satellite is ensured by choosing imagery over the same geographic area that is acquired 24 days apart (or multiples of 24 days apart). For each potential interferometric image pair, a baseline is estimated based on state vectors that describe the satellite orbit, slant range distance, and Doppler frequency. All the relevant information for a baseline estimation is retrieved from a scan results file in the ASF archive that is generated while ingesting raw telemetry signal into the processing system.

The baseline information is calculated on an image frame-by-frame basis. Baseline information is stored related to its orbit number that unambiguously determines the time of the acquisition. The interferometric baselines are stored separately for all InSAR capable beam modes, fine beam 1 (FN1) to fine beam

5 (FN5), and standard beam 1 (ST1) to standard beam 7 (ST7). For each beam mode, the orbits are organized by month and year of acquisition.

For each interferometric image pair, several parameters are provided. The sensor, the beam mode, the frame number, and the individual orbit numbers uniquely identify the two

image scenes of the pair. The orbit direction identifies whether the imagery is part of an ascending or descending orbit. The sequence numbers for the orbits simplify the ordering process of the data sets. The interferometric baseline is described spatially by its parallel and perpendicular component and by its temporal component, indicating how many days apart the two data sets have been acquired.

In addition to the Web pages the baseline information is available in two alternative formats that can be downloaded. First, the user can analyze the baseline information offline in tab delimited ASCII text files. Second, a more advanced way of searching interferometric baselines is provided by shape files that contain the location of the frame and the relevant data and baseline information as attribute tables. This allows the direct use of

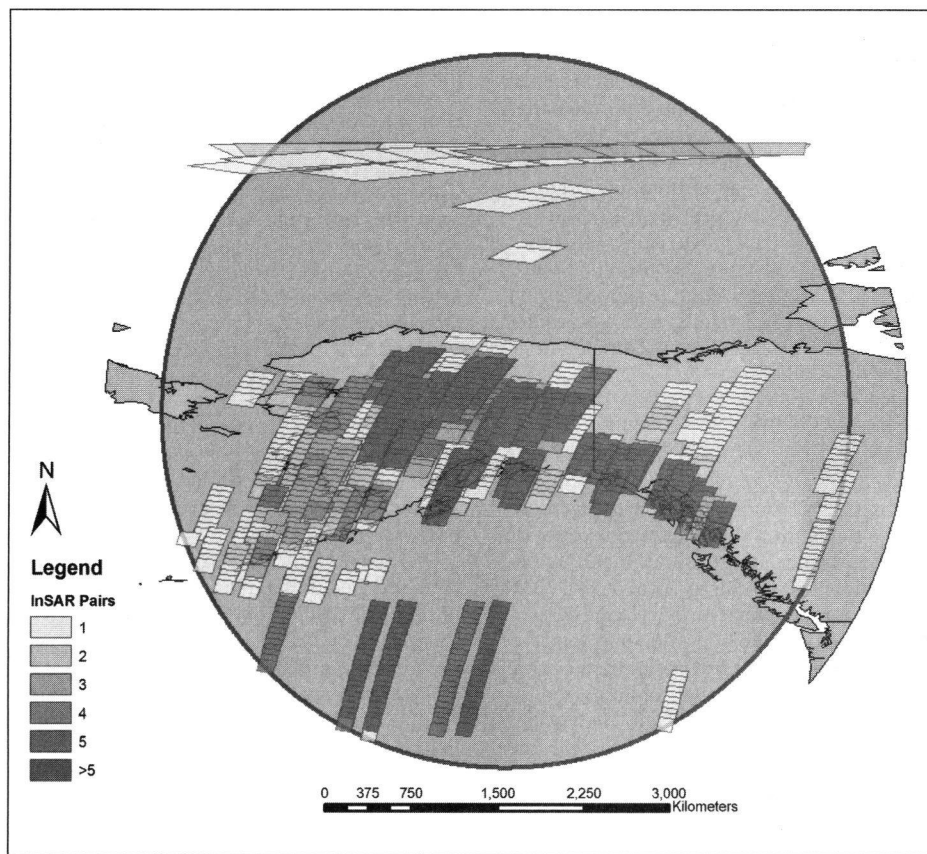


Fig. 1 Real-time RADARSAT-1 InSAR coverage for the ASF station mask. This figure shows an example of descending ST2 orbits with 24 days repeat cycle. The frames drawn on the map indicate areas where interferometric imagery is available. The color scheme represents how many image pairs have been acquired for a certain area. Original color image appears at the back of this volume.

Page 161

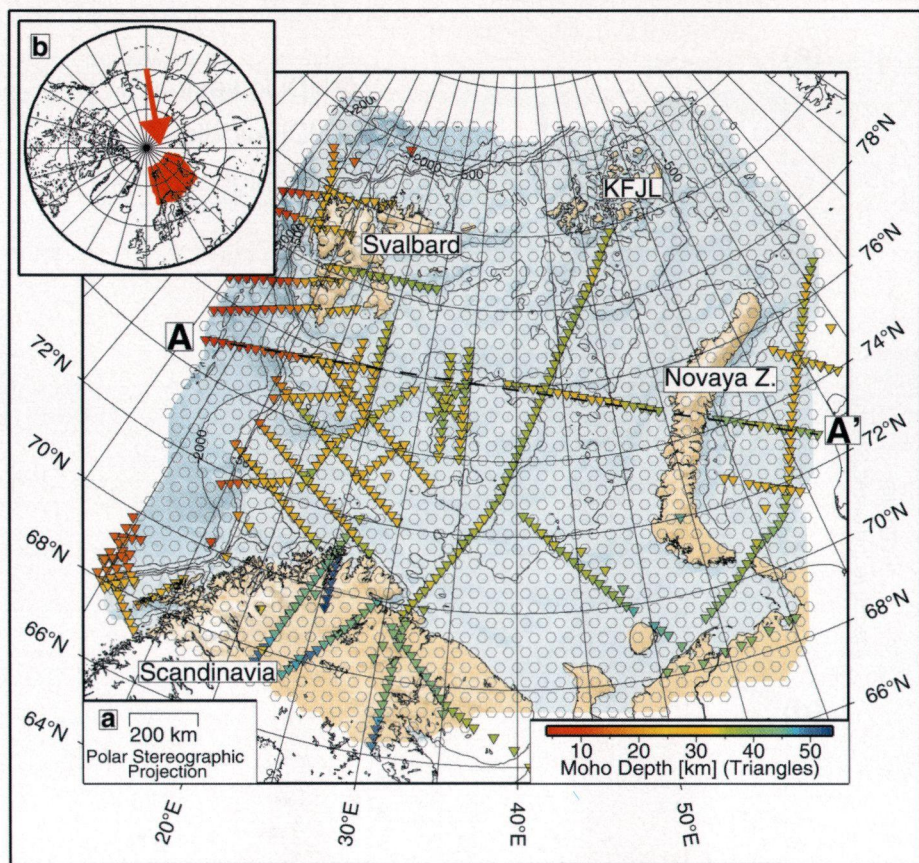


Fig. 1. Map of the greater Barents Sea region, shown in red in the inset map. The lines marked with triangles are wide-angle profiles where the color coding indicates the Moho depth. The small hexagons are tiles spaced 50 km apart that will be filled with crustal and upper mantle velocities. The profile A-A' is the one for which detailed results are shown in Figure 2. KFJL, Kaiser Franz Josef Land.

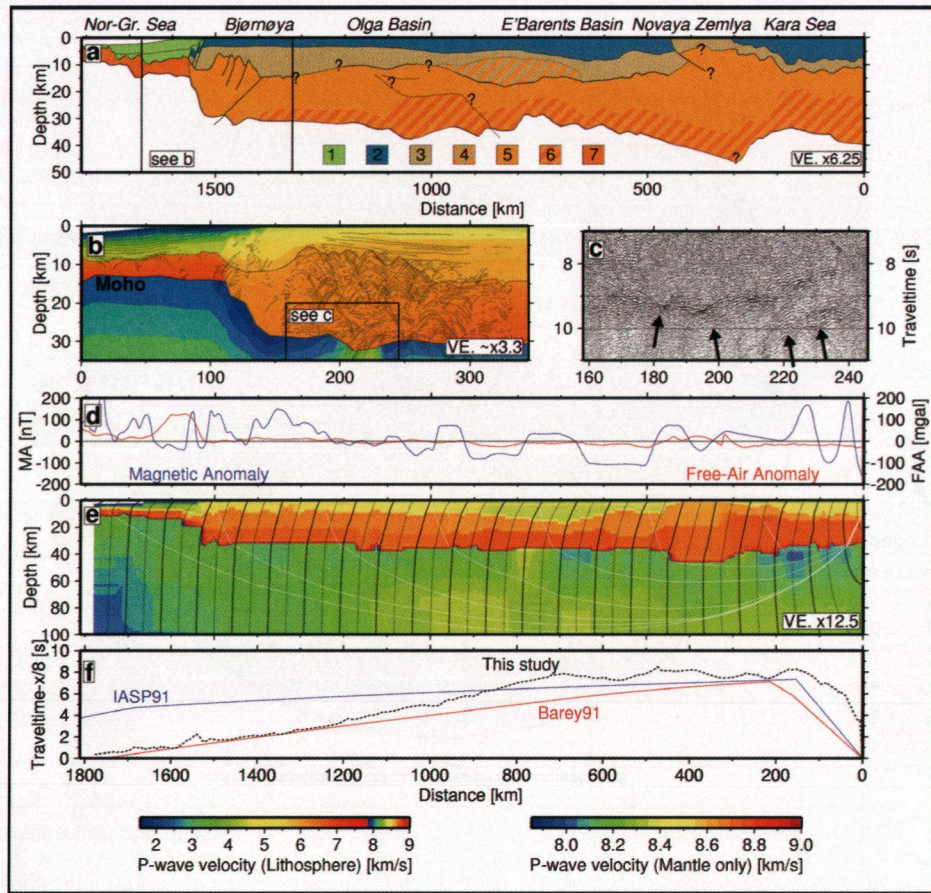


Fig. 2. Observations, interpretations, and modeling for the Barents Sea A-A' transect shown in Figure 1. Figure 2a shows the geological units along the transect ranging from the oceanic crustal domain in the very west to Novaya Zemlya and the Kara Sea in the east. Along the 1800-km-long transect, all available data were used to display the distribution of sedimentary and crystalline crustal rocks: 1, Cenozoic sediments; 2, Mesozoic sediments; 3, Paleozoic sediments; 4, Paleozoic sediments and/or crystalline rocks; 5, continental crystalline rocks; 6, lower crustal crystalline rocks with v_p 6.6–6.8 km/s; and 7, oceanic crystalline rocks. Figures 2b and 2c illustrate database examples along this transect, i.e., a P-wave velocity model (with line drawing) and deep seismic reflection data, respectively (see insert boxes for along-transect location). Figure 2d shows potential-field data along the profile, Figure 2e shows the 3-D model with superimposed seismic wave fronts, and Figure 2f shows travel times in comparison with two 1-D models. For the velocity models in Figures 2b and 2e, the lower color scales apply, where the left scale covers the entire range of lithospheric velocities and the right scale covers the mantle velocities only. Note that at 7.8 km/s, the scale shows repeating colors (crust-mantle transition).